Superluminal transmission of information through an electromagnetic metamaterial

Richard W. Ziolkowski*
Department of Electrical & Computer Engineering, The University of Arizona, 1230 E. Speedway, Tucson, Arizona 85721-0104
(Received 14 August 2000; published 23 March 2001)

A passive, matched two-time-derivative Lorentz material medium is designed to have its equivalent permittivity and permeability smaller than their values in free space over a large range of frequencies. Superluminal pulse propagation in this medium and consequent superluminal information exchange without a violation in causality are demonstrated. Additional properties of this medium are developed including the energy in it and the force characteristics induced on it by electromagnetic field interactions. It is shown that the force on the medium can be made to be attractive or repulsive using a change in frequency or a change in the material characteristics. Potential applications are discussed.

DOI: 10.1103/PhysRevE.63.046604 PACS number(s): 41.20.Jb, 03.50.De, 84.40.−x, 81.05.Zx

I. INTRODUCTION

In the past few years, there has been a renewed interest in using structures to develop materials that mimic known material responses or that qualitatively have new response functions that do not occur in nature. Artificial dielectrics [1] were explored, for example, in the 1950s and 1960s for lightweight microwave antenna lenses. Artificial chiral materials, e.g., [2–8], were investigated in the 1980s and 1990s for microwave radar absorber applications. Recent examples of these artificial material activities include photonic band-gap structured materials [9–13], artificial electric and magnetic molecules [14–19], and artificial electric and magnetic materials, which, like many of the chiral materials, can exhibit positive or negative permittivity or permeability properties [20–23]. Very recent experiments involving artificial materials with simultaneous negative permittivity and permeability [24,25] have captured the public's attention [26].

The qualitatively new response functions of these ''metamaterials'' are often generated by artificially fabricated, extrinsic, low-dimensional inhomogeneities. For instance, the artificial molecules are based upon the introduction of arrays of electrically small, loaded antennas into a host substrate. Design rules for obtaining the molecule metamaterials that exhibit the common Debye and Lorentz material model responses and their generalizations have been given for both electric and magnetic properties. They have already proven useful for Maxwell equation numerical simulation technologies [27–32].

In this paper, one of the metamaterial models, the two time derivative Lorentz material (2TDLM) model, will be emphasized. This model is a generalization of the standard Lorentz material model and encompasses the permittivity and permeability material responses experimentally obtained, for instance, in [25]. A 2TDLM medium slab that is matched to free space is designed, and its electromagnetic properties are explained. In particular, it will be shown that this type of 2TDLM medium can be designed so that it allows communication signals to propagate *in the medium* at speeds exceeding the speed of light in vacuum without violating causality. This 2TDLM medium is passive, and could be potentially realized physically. Simulations with a finite-difference time domain (FDTD) approach confirm the superluminal properties. The electromagnetic energy in and forces on a slab of this material are calculated for various values of the material's characteristic parameters.

It must be emphasized that these superluminal effects differ from the superluminal solutions of the wave equation [33,34] and their array/aperture realizations through the ''sling-shot'' effect [35] both acoustically [36] and electromagnetically [37]. These finite aperture experiments rely on a near-field effect; they do not violate causality since the resulting superluminal interference pattern surfs on a background of ''c'' traveling waves which arrive at the detector before the ''$>c$'' traveling interference peak does. On the other hand, the 2TDLM medium superluminal results are analogous to, but differ from the gain-assisted type of superluminal behavior discussed by Chiao and co-workers in [38–43] and illustrated more dramatically with recent experiments by Wang *et al.* [44]. Here the 2TDLM material is passive and is directly related to the double negative material realized in [25]. Moreover, the 2TDLM medium superluminal results are not related to a Cherenkov effect. Simply, as shown below, the 2TDLM medium parameters are selected to cause the natural speed of waves in it to be greater than ''c'' for a very large band of frequencies. The actual realization of this metamaterial would not violate causality. Since the artificial molecules depend on the condition that they be electrically small, the 2TDLM model becomes inappropriate at infinite frequencies. Because the discontinuity of turning on the communication signal requires those infinite frequencies, the leading edge of the signal is traveling at ''c'' and causality is preserved. This type of superluminal medium could, however, be used for a number of interesting applications including the propagation of signals along interconnects in integrated circuits (IC's) to increase their speeds.

The electromagnetic energy in and the forces induced on the 2TDLM medium by an electromagnetic field are characterized with the FDTD simulator. Issues of negative energy in a lossy dispersive medium that are associated with the resonance region are discussed. It is shown that the force induced on a 2TDLM medium can be attractive or repulsive depending on the 2TDLM parameters or on the frequency of

*Email address: ziolkowski@ece.arizona.edu

the interacting electromagnetic field. Potential applications and realizations of this result are discussed briefly.

II. 2TDLM MODEL PHYSICS

We are interested in the propagation effects through a medium that is linear and described by the 2TDLM model introduced in [14–17,27] and used in [31,32] to describe an absorbing material that could be matched to a lossy dielectric for use as an absorbing boundary condition in an FDTD simulator. The $\hat{x}$-directed polarization and $\hat{y}$-directed magnetization fields in such a material would have the forms

$$\frac{\partial^2}{\partial t^2}\mathcal{P}_x+\Gamma\frac{\partial}{\partial t}\mathcal{P}_x+\omega_o^2\mathcal{P}_x = \epsilon_o\left(\omega_p^2\chi_\alpha^e\mathcal{E}_x+\omega_p\chi_\beta^e\frac{\partial}{\partial t}\mathcal{E}_x+\chi_\gamma^e\frac{\partial^2}{\partial t^2}\mathcal{E}_x\right), \quad (1)$$

$$\frac{\partial^2}{\partial t^2}\mathcal{M}_y+\Gamma\frac{\partial}{\partial t}\mathcal{M}_y+\omega_o^2\mathcal{M}_y = \omega_p^2\chi_\alpha^m\mathcal{H}_y+\omega_p\chi_\beta^m\frac{\partial}{\partial t}\mathcal{H}_y+\chi_\gamma^m\frac{\partial^2}{\partial t^2}\mathcal{H}_y, \quad (2)$$

where ω_0 is the resonance frequency and $\Gamma^{e,m}$ is the width of that resonance. The terms $\chi_\alpha^{e,m}$, $\chi_\beta^{e,m}$, and $\chi_\gamma^{e,m}$ represent, respectively, the coupling of the electric (magnetic) field and its first and second time derivatives to the local electric (magnetic) dipole motions. The term ω_p can be viewed as the plasma frequency associated with those dipoles and is introduced to make the $\chi^{e,m}$ coefficients dimensionless. Assuming an $\exp(j\omega t)$ time variation, this 2TDLM model leads to the following frequency-domain electric and magnetic susceptibilities:

$$\chi_{xx}^e(\omega)=\frac{\tilde{P}_x(\omega)}{\epsilon_0\tilde{E}_x(\omega)}=\frac{\omega_p^2\chi_\alpha^e+j\omega\omega_p\chi_\beta^e-\omega^2\chi_\gamma^e}{-\omega^2+j\omega\Gamma^e+\omega_0^2}, \quad (3)$$

$$\chi_{yy}^m(\omega)=\frac{\tilde{M}_y(\omega)}{\tilde{H}_y(\omega)}=\frac{\omega_p^2\chi_\alpha^m+j\omega\omega_p\chi_\beta^m-\omega^2\chi_\gamma^m}{-\omega^2+j\omega\Gamma^m+\omega_0^2}. \quad (4)$$

Moreover, as was highly desired for the electromagnetic absorber applications, we will force the 2TDLM medium to be matched to free space. This means we set the electric and magnetic parameters to be the same to obtain $\chi_{xx}^e(\omega)=\chi_{yy}^m(\omega)=\chi_{2\mathrm{TDLM}}(\omega)$, where

$$\chi_{2\mathrm{TDLM}}(\omega)=\frac{\omega_p^2\chi_\alpha+j\omega\omega_p\chi_\beta-\omega^2\chi_\gamma}{-\omega^2+j\omega\Gamma+\omega_0^2}. \quad (5)$$

This guarantees that the wave impedance in this matched 2TDLM medium equals that of free space,

$$Z_{2\mathrm{TDLM}}=\left\{\frac{\mu_0[1+\chi_{2\mathrm{TDLM}}(\omega)]}{\epsilon_0[1+\chi_{2\mathrm{TDLM}}(\omega)]}\right\}^{1/2}=\left(\frac{\mu_0}{\epsilon_0}\right)^{1/2}=Z_0, \quad (6)$$

which means the reflection coefficient from it will be zero, i.e., $R=(Z_{2\mathrm{TDLM}}-Z_0)/(Z_{2\mathrm{TDLM}}+Z_0)=0$.

The 2TDLM model (5) recovers the standard Lorentz model when $\chi_\beta=\chi_\gamma=0.0$. It also recovers the electric plasmon behavior for the permittivity of the ''bed of nails'' medium discussed in [22] when $\omega_0=\chi_\beta=\chi_\gamma=0.0$, and the magnetic permeability response for the split ring resonator medium reported in [23] when $\chi_\alpha=\chi_\beta=0.0$.

More generally, consider the large frequency behavior of the susceptibility $\chi_{2\mathrm{TDLM}}(\omega)$. One obtains

$$\lim_{\omega\to\infty}\chi_{2\mathrm{TDLM}}(\omega)\sim\chi_\gamma. \quad (7)$$

This means, for instance, that the 2TDLM model's permittivity and permeability at high frequencies

$$\epsilon_{2\mathrm{TDLM}}(\infty)\sim\epsilon_0(1+\chi_\gamma), \qquad \mu_{2\mathrm{TDLM}}(\infty)\sim\mu_0(1+\chi_\gamma) \quad (8)$$

depend only on the value of χ_γ. On the other hand, one finds that the dc behavior of the 2TDLM susceptibility is

$$\lim_{\omega\to 0}\chi_{2\mathrm{TDLM}}(\omega)\sim\frac{\omega_p^2}{\omega_0^2}\chi_\alpha \quad (9)$$

so that the 2TDLM model's dc permittivity and permeability

$$\epsilon_{2\mathrm{TDLM}}(0)\sim\epsilon_0\left(1+\frac{\omega_p^2}{\omega_0^2}\chi_\alpha\right), \qquad \mu_{2\mathrm{TDLM}}(0)\sim\mu_0\left(1+\frac{\omega_p^2}{\omega_0^2}\chi_\alpha\right) \quad (10)$$

depend only on the value of χ_α.

In particular, we will be considering cases for which $\chi_\gamma<0$ so that, for instance, at high frequencies $\epsilon(\infty)/\epsilon_0<1$ and $\mu(\infty)/\mu_0<1$. Recall that the interest in this choice is driven by the realization of such parameter conditions in recent double negative metamaterial experiments [25]. This coefficient choice will define the superluminal 2TDLM media of interest here.

Figure 1 illustrates the real and imaginary values of $\chi_{2\mathrm{TDLM}}(\omega)$ for a medium with $\chi_\alpha=1.0$, $\chi_\beta=1.0\times10^{-5}$, $\chi_\gamma=-0.5$, $\Gamma=1.0\times10^{-1}\omega_0$, and $\omega_p=\omega_0=2\pi f_0$ for $f_0=1.0\times10^9$ Hz$=1.0$ GHz. These parameters are selected to illustrate with the real part of the susceptibility the ability of the 2TDLM model to realize large negative permittivity and permeability values near the resonance as well as permittivity and permeability values below their free-space values away from it. The large negative value for the imaginary part of the susceptibility at the resonance frequency illustrates that, like a Lorentz medium, the 2TDLM medium is very lossy near its resonance.

We will consider an x-polarized, one-dimensional plane wave propagating in the z direction in a semi-infinite matched 2TDLM slab. The dispersion relation in the 2TDLM medium is

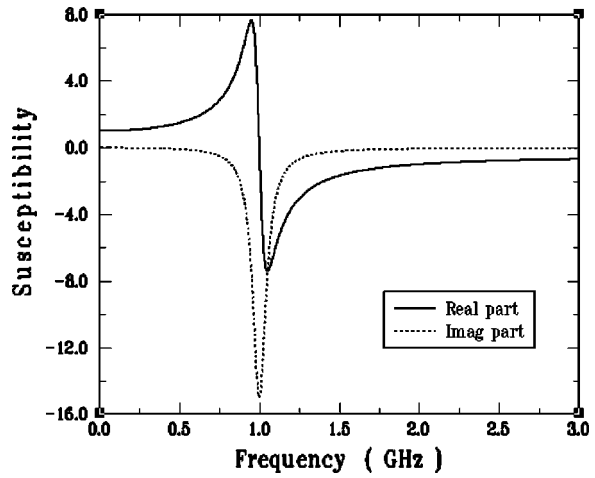

FIG. 1. Real and imaginary parts of the 2TDLM susceptibility with $\chi_\alpha = 1.0$, $\chi_\beta = 1.0\times 10^{-5}$, $\chi_\gamma = -0.5$, $\Gamma = 1.0\times 10^{-1}\omega_0$, and $\omega_p = \omega_0 = 2\pi f_0$ for $f_0 = 1.0\times 10^9$ Hz.

$$k^2 = \omega^2[\epsilon(\omega)\mu(\omega)] = \omega^2\epsilon_0\mu_0[1+\chi_{2\mathrm{TDLM}}(\omega)]^2, \quad (11)$$

which means the speed of the wave is

$$v(\omega) = \frac{1}{[\epsilon(\omega)\mu(\omega)]^{1/2}} = \frac{c}{|1+\chi_{2\mathrm{TDLM}}(\omega)|} \quad (12)$$

so that at frequencies well above the resonance one has

$$\lim_{\omega\to\infty} v(\omega) \sim \frac{c}{|1+\chi_\gamma|}. \quad (13)$$

Therefore, if $-2<\chi_\gamma<0$, this medium should exhibit superluminal speeds of propagation. The medium illustrated by Fig. 1 is such a case with speed $2c$ for frequencies well above f_0.

We note that the 2TDLM model characteristics can be realized with various artificial molecule arrangements of small dipole and loop antennas loaded with particular LRC combinations. Experimental efforts [21,23,25] have shown that it can also be realized with particular combinations of electric and magnetic structures. We note that the 2TDLM model characteristics can also be obtained as a combination of lower-order models [14,16,17]. For instance, a combined Debye and time derivative Debye material will produce a 2TDLM material. The more exotic time derivative Debye electric material could be realized with lossy, small conductive spheres embedded in a host substrate (see, for instance, [20], p. 484); the corresponding magnetic material could be realized with small, thin conducting shells (see, for instance, [20], p. 481). This combined lower-order model approach may be useful for realizations of the metamaterials; it is the approach that leads to the gain doublet used effectively in [40,44]. Note, however, that the form of the 2TDLM susceptibilities is opposite to those associated with the inverted medium superluminal investigations. For instance, from [38] the superluminal effects deal with the frequency response of the inverted medium near dc rather than near infinity, as is the case here.

III. SIMULATOR

To test these concepts, we used a standard 1D FDTD simulator that solves the electric, polarization, magnetic, and magnetization (EPHM) fields form of Maxwell's equations:

$$\epsilon_0\partial_t\vec{E} = +\nabla\times\vec{H} - \partial_t\vec{P},$$
$$\mu_0\partial_t\vec{H} = -\nabla\times\vec{E} - \mu_0\partial_t\vec{M} \quad (14)$$

using a staggered spatial grid, leap-frog-in-time algorithm [45,46]. This approach has been used successfully for several metamaterial investigations including those associated with the artificial molecules [14,19] and photonic band-gap structures [47].

For discussion purposes, we consider only the components E_x, P_x, H_y, M_y and propagation along the z direction. We then solve the following system numerically:

$$\epsilon_0\partial_t E_x = -\partial_z H_y - \partial_t P_x,$$
$$\mu_0\partial_t H_y = -\partial_z E_x - \mu_0\partial_t M_y, \quad (15)$$

where P_x and M_y satisfy the 2TDLM ordinary differential equations (1) and (2).

Using finite difference approximations to the derivatives, we obtain the electric and polarization field update equations:

$$\epsilon_0 E_x^{n+1}(i) + P_x^{n+1}(i) = \epsilon_0 E_x^n(i) + P_x^n(i) - \frac{\Delta t}{\Delta z}[H_y^{n+1/2}(i+1/2) - H_y^{n+1/2}(i-1/2)], \quad (16)$$

$$-\left[\frac{\epsilon_0\omega_p^2\Delta t^2}{2}\chi_\alpha + \frac{\epsilon_0\omega_p\Delta t}{2}\chi_\beta + \epsilon_0\chi_\gamma\right]E_x^{n+1}(i) + \left[1+\frac{\Gamma\Delta t}{2}+\frac{\omega_0^2\Delta t^2}{2}\right]P_x^{n+1}(i) = -2\epsilon_0\chi_\gamma E_x^n(i) + 2P_x^n(i) + \left[\frac{\epsilon_0\omega_p^2\Delta t^2}{2}\chi_\alpha - \frac{\epsilon_0\omega_p\Delta t}{2}\chi_\beta + \epsilon_0\chi_\gamma\right]E_x^{n-1}(i) - \left[1-\frac{\Gamma\Delta t}{2}-\frac{\omega_0^2\Delta t^2}{2}\right]P_x^{n-1}(i). \quad (17)$$

This can be written in matrix form, which is solved to give the semi-implicit update equations for the electric and polarization fields:

$$E_x^{n+1}(i)=\frac{A_{22}B_{11}-A_{12}B_{21}}{\det A}E_x^n(i)+\frac{A_{22}B_{12}-A_{12}B_{22}}{\det A}P_x^n(i)+\frac{A_{22}C_1-A_{12}C_2}{\det A},$$

$$P_x^{n+1}(i)=\frac{A_{11}B_{21}-A_{21}B_{11}}{\det A}E_x^n(i)+\frac{A_{11}B_{22}-A_{21}B_{12}}{\det A}P_x^n(i)+\frac{-A_{21}C_1+A_{11}C_2}{\det A}, \tag{18}$$

where the vector and matrix elements

$$A_{11}=\epsilon_0,$$

$$A_{12}=1,$$

$$A_{21}=-\epsilon_0\left[\frac{\omega_p^2\Delta t^2}{2}\chi_\alpha+\frac{\omega_p\Delta t}{2}\chi_\beta+\chi_\gamma\right],$$

$$A_{22}=1+\frac{\Gamma\Delta t}{2}+\frac{\omega_0^2\Delta t^2}{2},$$

$$B_{11}=\epsilon_0,$$

$$B_{12}=1,$$

$$B_{21}=-2\epsilon_0\chi_\gamma,$$

$$B_{22}=2,$$

$$C_1=-\frac{\Delta t}{\Delta z}[H_y^{n+1/2}(i+1/2)-H_y^{n+1/2}(i-1/2)],$$

$$C_2=\epsilon_0\left[\frac{\omega_p^2\Delta t^2}{2}\chi_\alpha-\frac{\omega_p\Delta t}{2}\chi_\beta+\chi_\gamma\right]E_x^{n-1}(i)-\left[1-\frac{\Gamma\Delta t}{2}-\frac{\omega_0^2\Delta t^2}{2}\right]P_x^{n-1}(i).$$

Because of the duality of their differential equations, the corresponding discretized magnetic and magnetization field equations follow immediately.

The Δz and Δt are related through the Courant-Friedrichs-Levy (CFL) condition [45]: $\Delta t=\gamma\Delta z/v_{\max}$, where $\gamma\leqslant 1$ and $v_{\max}$ is the maximum wave speed in the grid. Because we used $\chi_\gamma=-0.5$ to achieve a speed of $2c$ for all of the superluminal studies, the time step Δt was set to be $\Delta t=0.48\Delta z/c$, just slightly under the CFL condition requirements.

The FDTD grid was terminated at both ends with one-way wave operator absorbing boundary conditions (ABCs) [45] appropriate for the CFL number used in the simulations. This ABC is exact when $\gamma=1$.

The reason for using this second-order discretization scheme for the polarization and magnetization equations is that it has been widely used in dealing with dispersive media (see, for instance, [45], pp. 246–251). While other approaches are viable, this one is straightforward and simple to implement. One must, however, exercise some caution [48] in exploring numerically all of the available parameter space since there are many wave speeds present in this system and the CFL condition must be set appropriately to achieve a stable 2TDLM FDTD algorithm.

The initial field is launched from a total-field/scattered-field plane within the mesh [45]. Two types of unit amplitude pulses were used. One was a single-cycle, broad bandwidth pulse

$$f(t)=\begin{cases}\sqrt{7.0}(7.0/6.0)^3\left(\dfrac{t-T_p/2}{T_p/2}\right)\left[1-\left(\dfrac{t-T_p/2}{T_p/2}\right)^2\right]^3 & \text{for } 0\leqslant t\leqslant T_p\\ 0 & \text{for } t>T_p,\end{cases} \tag{19}$$

where T_p is the length of time the pulse has a nonzero value. This single-cycle pulse has a broad bandwidth; the peak of its frequency spectrum occurs at $f_{00}=1/T_p$. The other is the multiple cycle m-n-m pulse:

$$f(t)=\begin{cases}g_{\rm on}(t)\sin(\omega_{00}t) & \text{for } 0\leqslant t<mT_p\\ \sin(\omega t) & \text{for } mT_p\leqslant t\leqslant(m+n)T_p\\ g_{\rm off}(t)\sin(\omega_{00}t) & \text{for } (m+n)T_p<t\leqslant(m+n+m)T_p\\ 0 & \text{for } t>(m+n+m)T_p,\end{cases} \tag{20}$$

where $T_p=2\pi/\omega_{00}=1/f_{00}$ is the period of one cycle and the three-derivative smooth window functions

$$g_{\rm on}(t)=10.0x_{\rm on}^3-15.0x_{\rm on}^4+6.0x_{\rm on}^5,$$
$$g_{\rm off}(t)=1.0-[10.0x_{\rm off}^3-15.0x_{\rm off}^4+6.0x_{\rm off}^5], \tag{21}$$

where $x_{\rm on}=1.0-(mT_p-t)/mT_p$ and $x_{\rm off}=[t-(m+n)T_p]/mT_p$. The m-n-m pulse is a sinusoidal signal that has a smooth windowed turn-on for m cycles, a constant amplitude for n cycles, and then a smooth windowed turn-off for m cycles; hence, it has an adjustable bandwidth (through the total number of cycles $m+n+m$) centered at the frequency f_{00}. For all of the cases considered below, a 20-cycle, 2-16-2 pulse was used to probe the 2TDLM slab.

Unless otherwise noted, the 1D FDTD problem space for the simulation results discussed below was taken to be 8000

cells long, where $\Delta z = 1.0 \times 10^{-3} m = \lambda_s/300$, where the fixed frequency $f_s = c/\lambda_s = 1.0$ GHz. The corresponding time step was $\Delta t = 0.48 \Delta z/c = 1.6 \times 10^{-12}$ s $= 1.6$ ps. The total field/scattered field plane was set at $z = i\Delta z$, where $i = 1000$; the front face of the 2TDLM slab was set at $z = i\Delta z$, where $i = 3000$; and the back face of the 2TDLM slab was set at $z = i\Delta z$, where $i = 5000$. Thus, the 2TDLM slab was 2000 cells or 2.0 m thick.

IV. SIMULATION RESULTS

Several issues were investigated both analytically and numerically. These included the speed of propagation of signals in, the energy density in, and the forces induced on the matched 2TDLM slab. Each are considered separately below.

A. Faster than light propagation

To investigate the propagation of pulses in a medium with $\epsilon < \epsilon_0$ and $\mu < \mu_0$, a free-space matched 2TDLM slab with the parameters $\chi_\alpha = 1.0$, $\chi_\beta = 1.0 \times 10^{-5}$, $\chi_\gamma = -0.5$, $\Gamma = 1.0 \times 10^{-5} \omega_0$, and $\omega_p = \omega_0 = 2\pi f_0$ for $f_0 = 0.01$ GHz was considered. Note that this 2TDLM medium has a much narrower resonance than the one shown in Fig. 1, and that resonance is located at $f_0 = 0.01$ GHz. This choice allows a simple consideration of the maintenance of the shape of the pulse as it propagates in the 2TDLM slab without having to worry about the impact of the absorption near resonance. In fact, because most of its frequencies are well above the resonance frequency, a single-cycle pulse having a peak frequency $f_{00} = 1.0$ GHz should travel without distortion at a speed $2c$ in this slab.

To compare the superluminal results with the corresponding standard subluminal ones, we also considered the free-space matched 2TDLM slab with the parameters $\chi_\alpha = 1.0$, $\chi_\beta = 1.0 \times 10^{-5}$, $\chi_\gamma = +0.5$, $\Gamma = 1.0 \times 10^{-5} \omega_0$, and $\omega_p = \omega_0 = 2\pi f_0$ for $\omega_0 = 0.01$ GHz. In this 2TDLM slab, the frequencies well above the resonance travel at speed $c/2$.

The FDTD results for the propagation of a single-cycle pulse with its center frequency at 1.0 GHz in both 2TDLM slabs are shown in Fig. 2. The time histories of the electric field at a point ten cells beyond the 2TDLM slab's back interface (at $z = i\Delta z$ with $i = 5010$) are given. Also given for comparison purposes is the FDTD result at the same point for the same pulse propagating in free space. The peaks of the pulses are found to occur in time precisely at the values corresponding to the speeds in their respective media, i.e., analytically the neighboring peaks should be separated by $1000/0.48 \Delta t = 2083.33 \Delta t$; they are separated by $2084 \Delta t$ numerically.

The results for the superluminal 2TDLM slab do not violate causality (Einstein relativity). Simply, many electromagnetic waves travel faster than c in this medium. Moreover, the effect cannot occur until an initial pulse ''activates'' the 2TDLM medium. The waves are then exchanged between cells in the 2TDLM slab at their respective wave speeds. This dispersive effect is shown in Fig. 3. The electric fields $E_x(z,t)$ that propagate with the 2TDLM slab being present

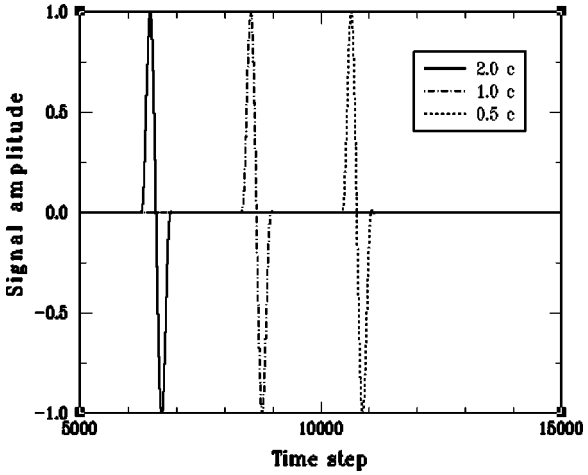

FIG. 2. Comparison of the propagation of a single-cycle pulse in a superluminal 2TDLM slab (solid line), a subluminal 2TDLM slab (dashed line), and in free space (dot-dashed line). These signals were measured at a point located 10 cells beyond the back-plane of the 2TDLM slab. The superluminal case illustrates that the medium parameters can be designed to insure that the pulse shape is preserved.

(solid curves) and without it (dashed curves) are given over the entire FDTD simulation space at three time values $t = 4.8$ ns $= 3000 \Delta t$ (curves to the left of cell number 3000), $t = 9.6$ ns $= 6000 \Delta t$ (curves between cell number 3000 and 5000), and $t = 16.0$ ns $= 10\,000 \Delta t$ (curves to the right of cell number 5000). The total field/scattered field, the front plane of the 2TDLM slab, and the rear plane of the 2TDLM slab are also shown. With these times, Fig. 3 shows the 2TDLM-case pulse before it interacts with the 2TDLM slab, while it is interacting with the 2TDLM slab, and after it interacts with the 2TDLM slab. One can see that before the 2TDLM slab, the free-space and 2TDLM-case pulses coincide.

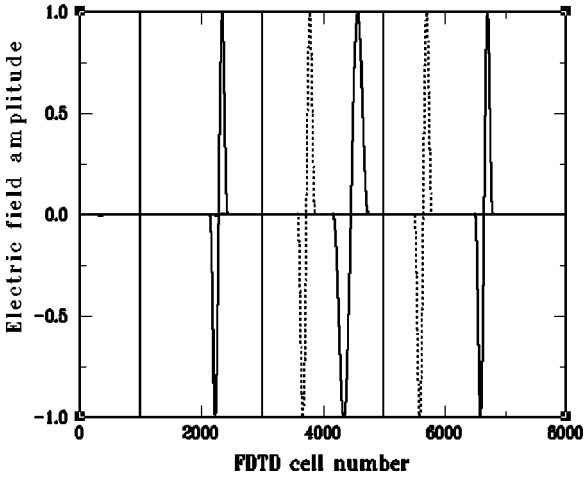

FIG. 3. The electric-field amplitude in the FDTD simulation space at the times $t = 4.8$ ns $= 3000 \Delta t$ (curves to the left of cell number 3000), $t = 9.6$ ns $= 6000 \Delta t$ (curves between cell number 3000 and 5000), and $t = 16.0$ ns $= 10\,000 \Delta t$ (curves to the right of cell number 5000). The solid lines represent the 2TDLM cases; the dashed lines represent the free-space cases.

Within the 2TDLM slab, one can see that the 2TDLM-case pulse has doubled its size in contrast to the free-space case due to the differing speeds of propagation of the frequency components that make up the pulse. Beyond the 2TDLM slab, one can see that the 2TDLM-case pulse, which has exited the superluminal medium, has reformed itself into the same shape as it had before entering the slab. The peaks of the free-space case pulse and the 2TDLM-case pulse are separated by 1000 cells as expected from the speed $2c$ inside the 2TDLM slab of the majority of the frequency components within the pulse. Note that there is a wave numerically reflected from the ''matched'' 2TDLM slab. It has a maximum amplitude that is 3.5×10^{-3} smaller than that of the incident pulse.

It is noted that essentially the same results are obtained for any 2TDLM slab that has $\chi_\gamma=-0.5$, has the same values for the products $\chi_\alpha\omega_p^2$ and $\chi_\beta\omega_p$, and has a narrow resonance, and for signals whose major frequency components are well above the resonance value. On the other hand, if the signal's frequency content is moved into the resonance region of the slab or vice versa, severe pulse distortion occurs. Few frequency components near f_0 propagate through the slab since most of their energy is absorbed in it. However, even in such cases, one can still observe the superluminal behavior for some of the highest frequency components of the pulse.

Finally, it must be recalled that since the artificial molecules are assumed electrically small in comparison to a wavelength to derive the metamaterial 2TDLM response, the 2TDLM model will break down in practice at very high frequencies. In fact, it is expected that as $\omega\rightarrow\infty$, $\epsilon\rightarrow\epsilon_0$, $\mu\rightarrow\mu_0$ for any realistic physical implementation of a 2TDLM metamaterial. Nonetheless, it is also expected that one can still realize a large band of frequencies over which this superluminal effect could be achieved.

To demonstrate that the speed at which information can be transmitted can be enhanced by the 2TDLM slab, signals consisting of a combination of single-cycle pulses were propagated through it. The basic information test signal consisted of two single-cycle pulses (19) with $f_{00}=1.0$ GHz that were separated in time by $2T_p$; i.e., two signal widths. This pulse could represent, for example, an on-off-off-on-off sequence of bits. The electric-field time histories measured at $z=5010\Delta z$ for this information test signal propagating in free space and propagating through the 2TDLM slab are shown in Fig. 4. Clearly the pulse shapes and distance between the pulses are maintained. The time of arrival of the pulses is enhanced by the presence of the superluminal 2TDLM slab; it provided the means for the transmission of information at speeds greater than those in free space.

A design of an experiment to confirm these matched 2TDLM slab results is currently in progress. Particular concerns include how well one can achieve the matched electric and magnetic properties in the same metamaterial. When considering scattering or simple propagation effects, one desires a matched material simply because the amplitudes of the transmitted signals will not be impacted by the interactions with the faces of the slab. Larger transmitted field values will generally be easier to detect. However, when considering information exchange via short pulses, a matched material is critical if one wants to minimize the impact of dispersion on the results. As noted previously, if the electric and magnetic properties of the 2TDLM metamaterial are identical at each frequency, the wave impedance at each frequency is the same. Consequently, the signals transmitted through such a matched 2TDLM metamaterial will experience no distortion. This effect is demonstrated in Fig. 4. If, on the other hand, the 2TDLM metamaterial is not matched and the electric and magnetic properties have significantly different dispersion characteristics, the shapes of the transmitted pulses will become severely distorted. This distortion could adversely affect the information exchange.

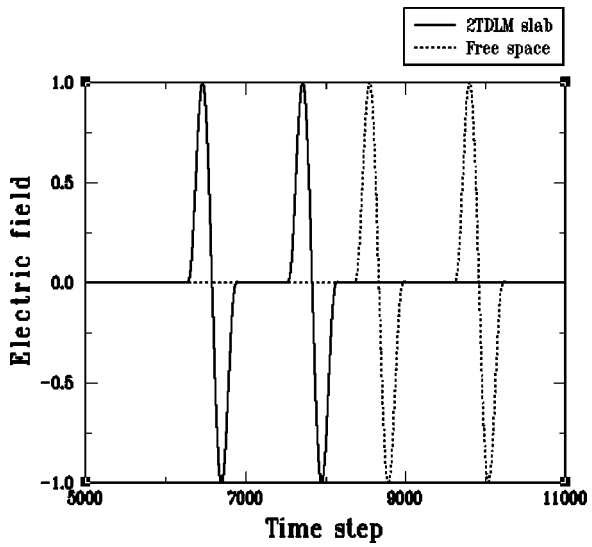

FIG. 4. Information can be transmitted at rates faster than in free space with the aid of the 2TDLM slab. The electric-field time history received at 10 cells beyond the back-plane of the 2TDLM slab is compared to its free-space propagating counterpart.

To test this behavior, the propagation of an information signal through a 2TDLM metamaterial derived as a variation of the one used in [25] was considered. The relative permittivity of the metallic rod portion of the 2TDLM metamaterial medium was set equal to

$$\epsilon_r(\omega)=1+\chi^e_{\exp}(\omega)=1-\frac{\omega_p^2}{\omega^2-j\Gamma^e\omega}, \tag{22}$$

where $\Gamma^e=0.1\omega_p$ with the plasma frequency $f_p=\omega_p/(2\pi)=3.618\times10^9$ Hz. The relative permittivity of the split ring resonator portion of the 2TDLM metamaterial medium was set equal to

$$\mu_r(\omega)=1+\chi^m_{\exp}(\omega)=1-\frac{F\omega^2}{\omega^2-j\Gamma^m\omega-\omega_0^2}, \tag{23}$$

where $F=+0.5$, $\Gamma^m=1.0\times10^{-5}\omega_0$ with the resonance frequency $f_0=\omega_0/(2\pi)=1.0\times10^9$ Hz. This choice gives a matching point $\epsilon_r(\omega_m)-1=\mu_r(\omega_m)-1$ at $f_m=\omega_m/(2\pi)$

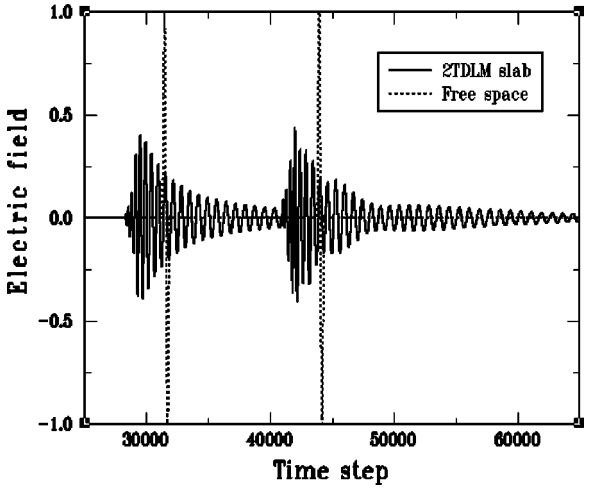

FIG. 5. Information can still be transmitted at rates faster than in free space with the aid of an unmatched ring-rod 2TDLM metamaterial slab. The electric-field time history received at 10 cells beyond the back-plane of the ring-rod 2TDLM slab is compared to its free-space propagating counterpart.

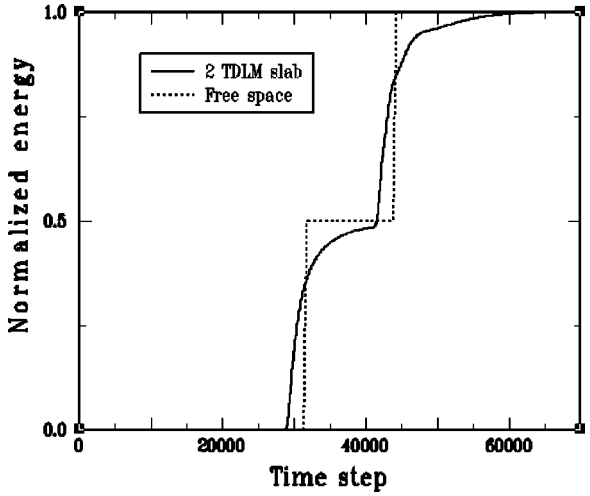

FIG. 6. The normalized energy received in time at a point 10 cells beyond the back-plane of the ring-rod 2TDLM slab is compared to its free-space propagating counterpart. More than 70% of the information energy is received at a rate faster than in free space with the aid of the ring-rod 2TDLM slab.

$=5.0\times10^{9}$ Hz that is above the lossy resonance region of the split ring resonator permeability and above cutoff for the metallic rod permittivity.

An information signal consisting of two single-cycle pulses (19), each with $f_{00}=1/T_p=5.0\times10^{9}$ Hz and separated in time by $20T_p$, was propagated numerically through this ring-rod 2TDLM metamaterial. Because of the higher frequencies involved, the FDTD cell size was modified to $\Delta z=2.0\times10^{-4}$. This maintained the disretization at $\lambda_{00}/300$. The time step $\Delta t=0.48\Delta z/c=3.2\times10^{-13}$ s$=0.32$ ps. The FDTD problem space size and the total number of time steps in the simulations were increased accordingly. The slab was taken to be 5000 FDTD cells thick. The electric field was measured again at the point located 10 FDTD cells beyond the back-plane of the 2TDLM slab. The FDTD results for the signal propagating through the ring-rod 2TDLM slab and through free space are compared in Fig. 5. Clearly there are severe distortions caused by dispersion as the signal propagates through the slab. These results also make it evident that the larger separation between the two single cycle pulses was chosen to achieve a distinction between the dispersed pulses, and that the slab was thinner (only 1.0 m thick) in order to minimize the amount of the dispersion on the signal.

Nonetheless, despite the distortions and the thinner medium, it is clear that the signal transmitted through the ring-rod 2TDLM slab does exhibit information exchange with enhanced speeds. If an intensity threshold detector measurement is used on these signals, it (barely) confirms this result. On the other hand, if the energy of each cycle is used to trigger the information exchange, the result is even more positive. The signal energy received at the observation point, as a function of time and normalized to the total energy received there, was also calculated. The FDTD results are shown in Fig. 6. More than 70% of the energy associated with each single-cycle pulse after it has propagated through the ring-rod 2TDLM slab is received at the detector before it would be if it propagated only in free space.

It is anticipated that in an actual experiment with its associated imperfections, a ring-rod 2TDLM slab may only marginally demonstrate the predicted enhanced information exchange. To achieve a more conclusive outcome, the current design process is exploring alternate metamaterial constructs to achieve experimental data more like the ideal simulation results shown in Fig. 4.

B. Electromagnetic energy

The question of determining the electromagnetic energy in a lossy dispersive medium was expected to be straightforward. However, upon review of the literature, it is not an easily answered question. To begin, the energy in a uniform, dispersionless medium is well known to be

$$U(t)=U_e(t)+U_m(t)=\int_V\left[\frac{1}{2}\epsilon|\vec{E}(\vec{r},t)|^2+\frac{1}{2}\mu|\vec{H}(\vec{r},t)|^2\right]dV. \tag{24}$$

The average total electromagnetic energy density would thus be

$$\langle U(t)\rangle=\langle U_e(t)\rangle+\langle U_m(t)\rangle. \tag{25}$$

It is immediately apparent that this form of the electromagnetic field energy would cause apparent problems if ϵ and μ were to take on negative values, as they could in dispersive media, since the energy would then be negative.

It is found that Eq. (24) must be changed in a lossless, dispersive medium [49–52]. The resulting time harmonic forms are

$$\langle U_e\rangle_\omega=\frac{1}{4}\int_V\{[\partial_\omega(\omega\epsilon(\omega))]\}|\vec{\tilde{E}}(\vec{r},\omega)|^2dV, \tag{26}$$

$$\langle U_m\rangle_\omega=\frac{1}{4}\int_V\{[\partial_\omega(\omega\mu(\omega))]\}|\vec{\tilde{H}}(\vec{r},\omega)|^2dV. \quad (27)$$

This handles the negative permittivity or permeability issue for normal test cases. For instance, for a lossless cold plasma, the permeability is a constant $\mu(\omega)=\mu_0$ and the permittivity

$$\epsilon(\omega)=\epsilon_0\left(1-\frac{\omega_p^2}{\omega^2}\right), \quad (28)$$

where ω_p is the plasma frequency. It is well known that $\epsilon(\omega)$ will be negative for $\omega<\omega_p$. The average electric- and magnetic-field energies are obtained with Eqs. (26) and (27) as

$$\langle U_e\rangle_\omega=\frac{\epsilon_0}{4}\int_V\left(1+\frac{\omega_p^2}{\omega^2}\right)|\vec{\tilde{E}}(\vec{r},\omega)|^2dV,$$
$$\langle U_m\rangle_\omega=\frac{\mu_0}{4}\int_V|\vec{\tilde{H}}(\vec{r},\omega)|^2dV, \quad (29)$$

which are both positive-definite quantities despite $\epsilon(\omega)$ taking on the negative values for $\omega<\omega_p$.

Regrettably, there are very few expressions available for lossy dispersive media such as the 2TDLM slab. The apparent problem with a choice of the energy density for lossy dispersive media becomes immediately apparent if one simply extends the above result as, for example,

$$\langle U_e\rangle_\omega=\frac{1}{4}\mathrm{Re}\int_V\{[\partial_\omega(\omega\epsilon(\omega))]\}|\vec{\tilde{E}}(\vec{r},\omega)|^2dV. \quad (30)$$

For a time harmonic plane wave at the resonance frequency, $f_{00}=f_0$, that is interacting with a very thin (length $=L$) 2TDLM slab, one obtains immediately the time-averaged electric-field energy

$$\langle U_e\rangle_{\omega_0}=\frac{1}{4}\epsilon_0\mathrm{Re}\left[\frac{\partial\omega\epsilon(\omega)}{\partial\omega}\right]_{\omega=\omega_0}|\vec{\tilde{E}}(\vec{r}_{\mathrm{slab}},\omega_0)|^2L$$
$$=\frac{1}{4}\epsilon_0\left[1+\frac{\omega_p\chi_\beta}{\Gamma}-2\left(\frac{\omega_p^2\chi_\alpha-\omega_0^2\chi_\gamma}{\Gamma^2}\right)\right]$$
$$\times|\vec{\tilde{E}}(\vec{r}_{\mathrm{slab}},\omega_0)|^2L. \quad (31)$$

For $\omega_p\equiv\omega_0$, this yields

$$\langle U_e\rangle_{\omega_0}=\frac{1}{4}\epsilon_0\left[1+\frac{\omega_0\chi_\beta}{\Gamma}-2\frac{\omega_0^2}{\Gamma^2}(\chi_\alpha-\chi_\gamma)\right]|\vec{\tilde{E}}(\vec{r}_{\mathrm{slab}},\omega_0)|^2L$$
$$=\frac{1}{4}\epsilon_0\left[1-2\frac{\omega_0^2}{\Gamma^2}\left(\chi_\alpha-\chi_\gamma-\frac{1}{2}\frac{\Gamma}{\omega_0}\chi_\beta\right)\right]$$
$$\times|\vec{\tilde{E}}(\vec{r}_{\mathrm{slab}},\omega_0)|^2L. \quad (32)$$

One finds that the energy density is easily made to be negative. In fact, consider a Lorentz medium that is recovered by setting $\chi_\beta=\chi_\gamma=0.0$. One obtains

$$\langle U_e\rangle_{\omega_0}^{\mathrm{Lorentz}}=\frac{1}{4}\epsilon_0[1-2(\omega_0^2/\Gamma^2)\chi_\alpha]|\vec{\tilde{E}}(\vec{r}_{\mathrm{slab}},\omega_0)|^2L. \quad (33)$$

This will be negative for any finite-width Lorentzian resonance line having $\chi_\alpha>(\Gamma/\omega_0)^2/2$. Similarly, in the special 2TDLM case for which $\chi_\alpha=\chi_\beta=0.0$, then

$$\langle U_e\rangle_{\omega_0}^{\mathrm{2TDLM}}=\frac{1}{4}\epsilon_0[1+2(\omega_0^2/\Gamma^2)\chi_\gamma]|\vec{\tilde{E}}(\vec{r}_{\mathrm{slab}},\omega_0)|^2L. \quad (34)$$

Therefore, the average energy density will be positive if $\chi_\gamma>0$ and will be negative if $\chi_\gamma<-(\Gamma/\omega_0)^2/2$. For a narrow resonance, i.e., for $\Gamma\ll\omega_0$, this will occur essentially if simply $\chi_\gamma<0$. For the more complicated narrow-resonance 2TDLM case that we have been considering, which has $\chi_\alpha=1.0$, $\chi_\beta=10^{-5}$, $\chi_\gamma=-0.5$, and $\Gamma=10^{-5}\omega_0$ with $\omega_p=\omega_0$, then the energy density could be quite large and negative at the resonant frequency: $\langle U_e\rangle_{\omega_0}\sim-10^{+10}\epsilon_0|\vec{\tilde{E}}|^2L/4$.

In view of these negative energy considerations, a more exact calculation was found for a lossy, temporally dispersive, spatially nondispersive medium [60]. In particular, if one defines the dispersion function as

$$D(k,\omega)=\omega\epsilon(\omega)-\frac{k^2}{\omega}\mu(\omega), \quad (35)$$

then for ω real and k complex, the real and imaginary parts of k being obtained from the dispersion relation $D(k,\omega)=0$, the averaged stored electromagnetic field energy becomes [[60], Eq. (22)]

$$\langle U\rangle_\omega=\frac{1}{4}\mathrm{Re}\left[\frac{\partial D}{\partial\omega}-jk_{Im}\frac{\partial^2D}{\partial\omega\partial k}\right.$$
$$\left.+2j\Gamma\left(j\frac{\partial D}{\partial\Gamma}\right)^{1/2}\frac{\partial}{\partial\omega}\left(j\frac{\partial D}{\partial\Gamma}\right)^{1/2}\right]|\vec{\tilde{E}}(\vec{r}_{\mathrm{slab}},\omega)|^2L, \quad (36)$$

where Γ again characterizes the width of the resonance. This formula was evaluated using MATHEMATICA™ for the superluminal 2TDLM slab case. The normalized average energy results $4\langle U\rangle_\omega/[|\vec{\tilde{E}}(\vec{r}_{\mathrm{slab}},\omega)|^2L]$, obtained with Eq. (26) are compared with those obtained with Eq. (36) in Fig. 7. One finds that Eq. (36) also predicts negative energies in a strong resonance region. There are clear differences between these two results caused by taking into account the width of the resonance, but the large negative value at the resonance frequency, where the absorption and the derivative of the permittivity are maximum, is not avoided even with this more detailed calculation.

Consequently, we are left at the moment without a definitive answer to our original question as to the correct value of the electromagnetic energy in the superluminal 2TDLM slab. Is having a negative electromagnetic energy result unphysi-

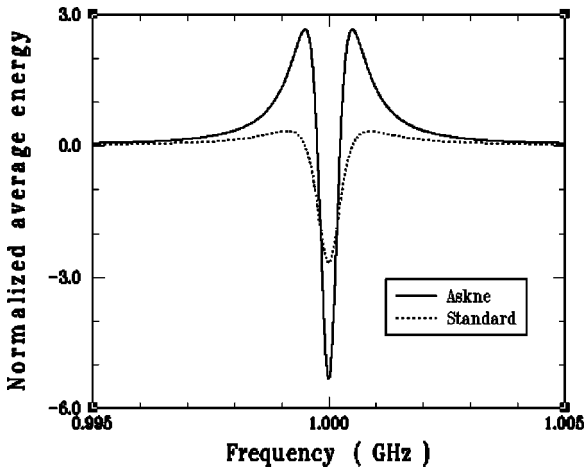

FIG. 7. The normalized average energy in the superluminal 2TDLM slab calculated with the dispersive medium expression, Eq. (26), and the lossy medium one, Eq. (36).

cal, especially in a resonance situation? It is noted that similar issues of negative energy and superluminal speeds have surfaced in some previous discussions regarding the Casimir effect [53–59]. Whether negative energy is semantics or a meaningful quantity has not been fully put to the test since the values associated with the Casimir effect are quite small. However, they could be investigated with one of the metamaterial constructs proposed here.

Since any quantity of interest could in principle be calculated with the FDTD simulator, several energy quantities were considered. We note that only the electromagnetic field energy issues will be discussed; thermodynamic arguments, which would require more information such as the mechanical stresses and the heat dissipation, are not included.

From Poynting's theorem, we know that the electromagnetic power flow through a surface $\mathcal{S}=\partial V$, which bounds the volume V and has the outward-pointing normal vector field $\vec{n}_{\mathcal{S}}$, in the EPHM formulation is given by the expression

$$\begin{aligned} &-\oint_{\mathcal{S}} d\mathcal{S}\vec{n}_{\mathcal{S}}\cdot\vec{S}(\vec{r},t) \\ &\quad=\partial_t\left\{\frac{1}{2}\int_V dV[\epsilon_0|\vec{E}(\vec{r},t)|^2+\mu_0|\vec{H}(\vec{r},t)|^2]dV\right\} \\ &\qquad+\int_V[\vec{E}(\vec{r},t)\cdot\partial_t\vec{P}(\vec{r},t)+\mu_0\vec{M}(\vec{r},t)\cdot\partial_t\vec{H}(\vec{r},t)]dV \\ &\quad=\mathcal{P}_{\text{fields}}+\mathcal{P}_{\text{dipoles}}, \end{aligned} \tag{37}$$

where Poynting's vector $\vec{S}(\vec{r},t)=\vec{E}(\vec{r},t)\times\vec{H}(\vec{r},t)$. Thus, propagating a wave through the 2TDLM slab, one finds that the total average energy lost to the slab over a time T would be given by the expression

$$\langle\mathcal{P}_{\text{total}}\rangle T=\int_0^T dt[\mathcal{P}_{\text{fields}}+\mathcal{P}_{\text{dipoles}}]. \tag{38}$$

In all of the 2TDLM cases considered numerically, this average energy/power quantity was positive. Thus, the energy transferred from the field to the slab was always positive.

On the other hand, returning to the standard electromagnetic field energy expressions, we set

$$U_{\text{fields}}(t)=\frac{1}{2}\int_V dV[\epsilon_0|\vec{E}(\vec{r},t)|^2+\mu_0|\vec{H}(\vec{r},t)|^2]dV, \tag{39}$$

$$U_{\text{dipoles}}(t)=\frac{1}{2}\int_V dV[\vec{P}(\vec{r},t)\cdot\vec{E}(\vec{r},t)+\mu_0\vec{M}(\vec{r},t)\cdot\vec{H}(\vec{r},t)], \tag{40}$$

$$U_{\text{total}}(t)=U_{\text{field}}(t)+U_{\text{dipoles}}(t). \tag{41}$$

These quantities were taken to represent the energy of the fields, the dipoles, and their total in the 2TDLM slab. For the numerical cases considered, they took the form

$$U_{\text{fields}}(t)=\frac{1}{2}\int_{\text{slab}} dz[\epsilon_0|E_x(z,t)|^2+\mu_0|H_y(z,t)|^2], \tag{42}$$

$$U_{\text{dipoles}}(t)=\frac{1}{2}\int_{\text{slab}} dz[P_x(z,t)E_x(z,t)+\mu_0 M_y(z,t)H_y(z,t)], \tag{43}$$

and were discretized appropriately. The average energies over a time $T=N\Delta t$ were simply taken to be

$$\langle U_{\text{fields}}\rangle=\frac{1}{T}\int_0^T dt U_{\text{fields}}(t), \tag{44}$$

$$\langle U_{\text{dipoles}}\rangle=\frac{1}{T}\int_0^T dt U_{\text{dipoles}}(t), \tag{45}$$

$$\langle U_{\text{total}}\rangle=\langle U_{\text{fields}}\rangle+\langle U_{\text{dipoles}}\rangle. \tag{46}$$

Clearly in all cases the average field energy should be positive; it was found to be positive in all of the numerical cases considered. On the other hand, the average dipole energies could become negative above the resonance. In particular, consider, for example, the time harmonic value of the average energy density stored in the electric dipoles in the 2TDLM case. One has

$$\frac{1}{2}\mathrm{Re}[\tilde{P}_x(\omega)\tilde{E}_x^*(\omega)]=\frac{1}{2}\epsilon_0|\tilde{E}_x(\omega)|^2\mathrm{Re}[\chi_{2\mathrm{TDLM}}(\omega)]=\frac{1}{2}\epsilon_0|\tilde{E}_x(\omega)|^2\frac{(\omega_p^2\chi_\alpha-\omega^2\chi_\gamma)(\omega_0^2-\omega^2)+\omega^2\omega_p\Gamma\chi_\beta}{(\omega_0^2-\omega^2)^2+\omega^2\Gamma^2}. \quad (47)$$

Setting $\omega\sim\omega_0+\delta$ with $\delta\ll 1$ and $\omega_p=\omega_0$ gives

$$\frac{1}{2}\mathrm{Re}[\tilde{P}_x(\omega)\tilde{E}_x^*(\omega)]\sim\frac{1}{2}\epsilon_0\omega_0|\tilde{E}_x(\omega+\delta)|^2 \times\frac{-2\delta(\chi_\alpha-\chi_\gamma)+\Gamma\chi_\beta}{4\delta^2+\Gamma^2}. \quad (48)$$

With $\Gamma\ll\omega_0$ and $\chi_\beta\ll 1$, the average dipole energy in a thin slab would be

$$\langle U_{\mathrm{dipole}}\rangle_{\omega+\delta}\sim-\frac{\delta\omega_0(\chi_\alpha-\chi_\gamma)}{\Gamma^2}\epsilon_0|\tilde{E}_x(\omega+\delta)|^2L \quad (49)$$

and, if $\chi_\alpha>\chi_\gamma$, it is negative (positive) slightly above (below) the resonance where $\delta>0$ ($\delta<0$). On the other hand, for $\omega\to\infty$,

$$\langle U_{\mathrm{dipole}}\rangle_\infty=\chi_\gamma\left[\frac{1}{2}\epsilon_0|\tilde{E}_x(\infty)|^2L\right]. \quad (50)$$

This is clearly positive or negative depending on the sign of χ_γ. Numerically, it was found that the average dipole energy was indeed negative in the regions where $\mathrm{Re}(\chi_{2\mathrm{TDLM}})<0$.

The remaining issue, which was addressed numerically, was the average total electromagnetic energy $\langle U_{\mathrm{total}}\rangle$ in the 2TDLM slab. As summarized in Table I, it was found to be negative for frequencies above and near the resonance frequency where $\mathrm{Re}(\chi_{2\mathrm{TDLM}})<-1$.

It is noted that in the case of the inverted media [42] or for the Casimir effect [59] studies, the change in the energy affected by the presence of the medium/structure was measured by calculating $-\langle U_{\mathrm{dipole}}\rangle$ (see also [61]). In both of those cases, this change of energy was positive, i.e., the potential energy was positive rather than negative. Thus, as with the metamaterial superluminal 2TDLM slab case, having a large enough negative susceptibility led to energies and forces opposite to those found in ''normal'' media.

To examine further the energy behavior over time, the electric-field distribution in the FDTD simulation space for the superluminal 2TDLM slab with the resonance frequency $f_0=1.0$ GHz is given in Fig. 8, for an incident 2-16-2 pulse with frequency $f_{00}=1.5$ GHz, at the times $t=20$ ns [Fig. 8(a); 12 500 time steps], $t=32$ ns [Fig. 8(b); 20 000 time steps], and $t=44$ ns [Fig. 8(c); 27 500 time steps]. For all of these times, the incident field is interacting with the 2TDLM slab. The small-amplitude waves to the left of the 2TDLM slab early in time ($t=20$ ns) represent the numerically reflected field that has the frequency $f=1.5$ GHz and later ($t=32$ ns and $t=44$ ns) represent the reradiated field that has frequencies centered about $f=1.0$ GHz. The fields to the right of the 2TDLM slab represent early in time the transmitted field and then later in time the energy being reradiated as the dipoles ring down. A Fourier transform of the field transmitted earlier in time shows, as expected, a very strong absorption of the frequencies surrounding the resonance, and later in time shows the dipoles ringing down.

TABLE I. Summary of FDTD simulator results for the energy in and force on the superluminal 2TDLM slab interacting with a 2-16-2 incident pulsed plane wave.

f_{00}	Dipole energy	Total energy	$\epsilon/\epsilon_0,\mu/\mu_0$	Force
0.5×10^9	>0	>0	>1	>0
1.0×10^9	<0	>0	>1	>0
1.5×10^9	<0	<0	<0	>0
10.0×10^9	<0	>0	$>0,<1$	<0

Note that for the given parameters, almost all of the absorbed energy is radiated to the right of the 2TDLM slab. This was confirmed by calculating the percent of the total incident energy (time-integrated Poynting vector, $\int_0^T dtS_z$) collected one cell in front of the 2TDLM slab and the transmitted energy collected one cell behind it. This result for an incident 2-16-2 pulse again having the frequency $f_{00}=1.5$ GHz that is transmitted through the superluminal 2TDLM slab with $f_0=1.0$ GHz is shown in Fig. 9. Note that the delay in the appearance of the reradiated energy occurs because the speed of the pulse (12) in the 2TDLM slab is much slower than c at this frequency. This slow wave speed behavior is further apparent in Fig. 8.

C. Electromagnetic force

Another issue investigated with the FDTD simulator was the calculation of the average force on the 2TDLM slab when a pulsed plane wave is interacting with it. The use of the forces exerted by electromagnetic waves to move small dielectric bodies (atoms, small spheres) has been studied for many years and has led to a number of practical applications (see, for instance, [62–66] and the references therein). The expression for the electromagnetic force density on a general stationary EPHM medium was found to have the form [67,68]

$$\vec{f}=(\vec{P}\cdot\vec{\nabla})\vec{E}+(\mu_0\vec{M}\cdot\vec{\nabla})\vec{H}+\partial_t\vec{P} \times(\mu_0\vec{H})-\partial_t(\mu_0\vec{M})\times(\epsilon_0\vec{E}). \quad (51)$$

Since we are dealing with 1D plane-wave scattering from a matched 2TDLM slab of thickness $L=\ell\Delta z$, the instantaneous total force becomes

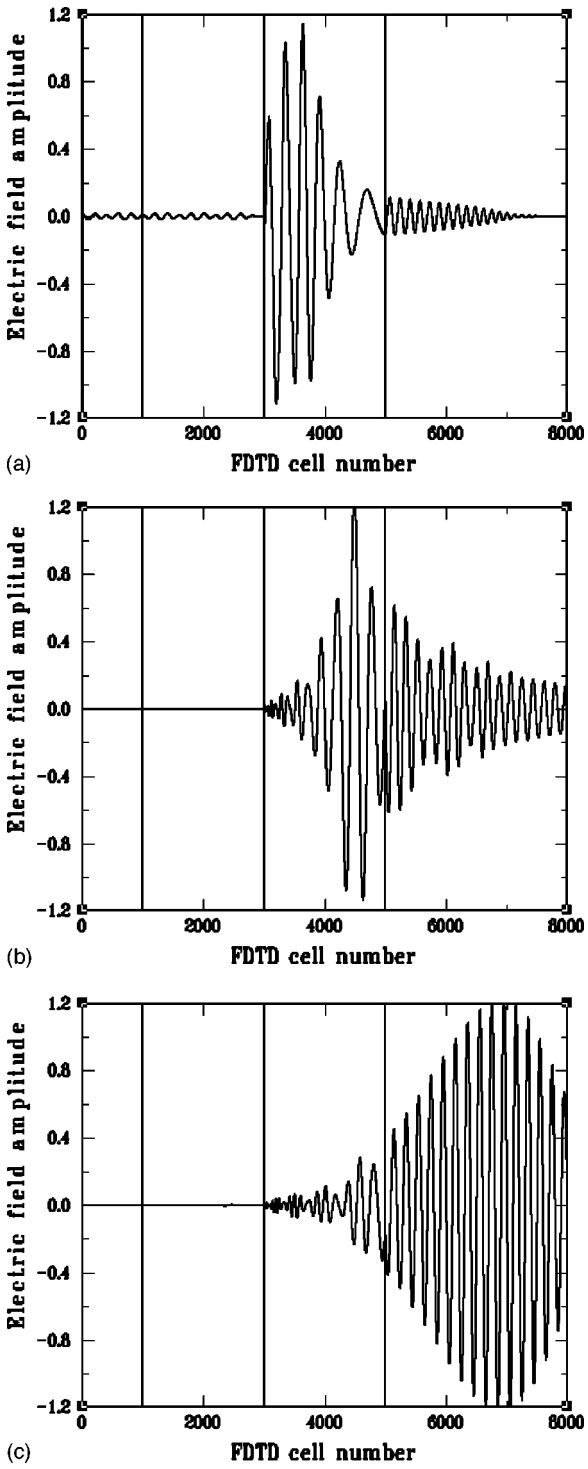

FIG. 8. The electric-field distribution in the FDTD simulation space for the superluminal 2TDLM slab with $f_0=1.0$ GHz at (a) $t=20$ ns, (b) $t=32$ ns, and (c) $t=44$ ns.

$$F_z(t)=\int_0^L dz\{[\partial_t P_x(z,t)]\mu_0 H_y(z,t)+\epsilon_0 E_x(z,t)\times[\partial_t \mu_0 M_y(z,t)]\}. \tag{52}$$

This force expression was implemented directly with the FDTD simulator in the discretized form

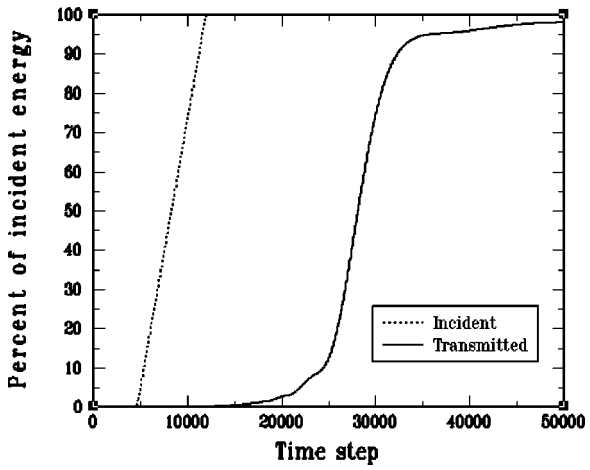

FIG. 9. The time-integrated power (energy) transmitted into and the power transmitted through the superluminal 2TDLM slab as a function of the number of FDTD time steps.

$$F_z^n=\sum_{i=1}^{i=\ell}\frac{\Delta z}{2\Delta t}\{\mu_0[P_x^{n+1}(i)-P_x^n(i)][H_y^{n+1/2}(i+1/2)+H_y^{n+1/2}(i-1/2)]+\epsilon_0\mu_0[M_y^{n+1/2}(i+1/2)-M_y^{n-1/2}(i+1/2)][E_x^n(i+1)+E_x^n(i)]\}. \tag{53}$$

For a pulse $N_p\Delta t$ long, the average force over the time $T=N\Delta t$ was calculated simply as

$$\langle F_z\rangle=\frac{1}{N}\sum_{n=1}^{n=N}F_z^n. \tag{54}$$

The average electromagnetic force was calculated for the interaction of single- and multiple-cycle plane wave pulses with the superluminal 2TDLM slab whose parameters $\chi_\alpha=1.0$, $\chi_\beta=1.0\times10^{-5}$, $\chi_\gamma=-0.5$, $\Gamma=1.0\times10^{-5}\omega_0$, and $\omega_p=\omega_0=2\pi f_0$ for $f_0=1.0$ GHz. The force and the corresponding energy results for the 2-16-2 pulse interactions with this 2TDLM slab are listed in Table I.

For the multiple-cycle pulse, it was found that the sign of the average force $\langle F_z\rangle$ corresponded most closely to the relative permittivity and permeability values. When both were positive and greater than 1, the average force was found to be repulsive. This was expected since the force on a dielectric particle is away from the source [65]. On the other hand, when both were negative, the average force was again repulsive. This is opposite to the prediction given in [24]. In this very absorptive region, the gradient force should dominate the scattering force so that the force should be $F_z\sim-\partial_z U_{\text{total}}$, which is repulsive as was found. However, when both the relative permittivity and permeability were positive but less than 1, the average force was found to be attractive. For the $f_{00}=1.5$ GHz case, the average force in the z direction over the 20-cycle 2-16-2 pulse was found to be $\sim+3.0$ pN; for the $f_{00}=10.0$ GHz case, it was ~-1.5 pN. Thus by changing the frequency of the incident pulse, the force on the 2TDLM slab could be made to be repulsive or attractive.

It is noted that these force results are analogous to, but opposite, the parelectric results given in [42,43]. As noted previously, the polarizability relationships between the inverted medium and dc permittivities considered there are opposite to the passive, high-frequency permittivity (and permeability) issues considered here.

Similar responses were obtained for the single-cycle pulses whose center frequencies coincided with the indicated narrowband ones. The only difference was in the sign of the total energy for the $f_{00}=1.5$ GHz case, where it was positive rather than negative. There were more frequencies with total energy values above zero than there were below zero. Moreover, the size of the energies and the average force were slightly smaller than the corresponding multiple-cycle pulse values in all trials, but their values were more uniform over the duration of the single-cycle pulse.

The corresponding subluminal 2TDLM slab with $\chi_\gamma = +0.5$ yielded a repulsive force for all of the indicated frequency values. Thus, because the practical artificial molecule realization of a 2TDLM slab could provide a means of changing the coefficient χ_γ in real time, one could effectively change the direction a force would act on a 2TDLM slab in two ways: (i) by varying the frequency of the input wave or (ii) by working above resonance and changing the value of χ_γ. One could then use a 2TDLM coating of some object in a zero-G environment (where even small forces are not insignificant) and move that object with a microwave beam either tuned to the appropriate frequencies or by reconfiguring the material characteristics appropriately.

V. CONCLUSIONS

An FDTD simulator was used to model the propagation of pulses through a 2TDLM medium. A free-space matched 2TDLM slab was designed to give distortion-free, superluminal speeds of propagation over a large band of frequencies. Single- and multiple-cycle pulses were used to test the signal propagation characteristics through the slab. The consequent electromagnetic energy in the 2TDLM slab and the electromagnetic force induced on it were calculated.

It was demonstrated that the speed at which information can be transmitted can be significantly enhanced with the introduction of the superluminal 2TDLM medium. It was also demonstrated that the electromagnetic energy in the superluminal 2TDLM medium is negative for a large band of frequencies above the resonant frequency. It was further demonstrated that the electromagnetic force induced on the 2TDLM slab can be made to be either attractive or repulsive. This force property depended on the material parameters or the frequency of the incident electromagnetic plane wave.

As was demonstrated, some of the superluminal properties modeled here could be tested with a variation of the double negative ring-rod metamaterial reported in [25]. However, because of the mismatch between the dispersion properties of the electric and magnetic components of such a 2TDLM metamaterial, information pulses propagated in it experience large distortions. Hence, improvements in the design of an experimentally viable 2TDLM metamaterial need to be made. In particular, construction of a matched 2TDLM metamaterial with the properties proposed here would lead one to a more definitive experiment. A variety of artificial molecule and alternative embedded structure metamaterials are currently being considered with the hope of fielding such a proof-of-principle experiment in the near future.

ACKNOWLEDGMENT

This work was supported in part by the Air Force Office of Scientific Research, Air Force Materiel Command, USAF, under Grant No. F49620-96-1-0039.

[1] R. E. Collin, *Field Theory of Guided Waves*, 2nd ed. (IEEE Press, Piscataway, NJ, 1990), pp. 749–786.
[2] D. L. Jaggard, A. R. Mickelson, and C. H. Papas, J. Appl. Phys. **18**, 211 (1979).
[3] D. L. Jaggard and N. Engheta, Electron. Lett. **25** (3), 173 (1989).
[4] D. L. Jaggard and N. Engheta, Electron. Lett. **26** (17), 1332 (1990).
[5] M. M. I. Saadoun, Ph.D. dissertation, University of Pennsylvania, 1992.
[6] I. V. Lindell, A. H. Sihvola, S. A. Tretyakov, and A. J. Vitanen, *Electromagnetic Waves in Chiral and Bi-isotropic Media* (Artech House, Boston, 1994), pp. 8–14.
[7] F. Mariotte, S. A. Tretyakov, and B. Sauviac, Microwave Opt. Technol. Lett. **7** (18), 861 (1994).
[8] *Proceedings of the Chiral '94 Workshop, 3rd International Workshop on Chiral, Bi-isotropic and Bi-anisotropic Media, Perigueux, France, 1994*, edited by F. Mariote and J.-P. Parneix (CEA-CESTA and PIOM Laboratory, Bordeaux, 1994).
[9] E. Yablonovitch, Phys. Rev. Lett. **58**, 2059 (1987).
[10] E. Yablonovitch and T. J. Gmitter, Phys. Rev. Lett. **63**, 1950 (1989).
[11] P. Villeneuve and M. Piche, Phys. Rev. B **46**, 4969 (1992).
[12] D. Maystre, Pure Appl. Opt. **3**, 975 (1994).
[13] J. D. Joannopoulos, R. D. Meade, and J. N. Winn, *Photonics Crystals: Molding the Flow of Light* (Princeton University Press, Princeton, NJ, 1995).
[14] R. W. Ziolkowski and F. Auzanneau, J. Appl. Phys. **82**, 3195 (1997).
[15] R. W. Ziolkowski and F. Auzanneau, J. Appl. Phys. **82**, 3192 (1997).
[16] F. Auzanneau and R. W. Ziolkowski, J. Phys. III **7**, 2405 (1997).
[17] F. Auzanneau and R. W. Ziolkowski, J. Electromagn. Waves Appl. **12**, 353 (1998).
[18] F. Auzanneau and R. W. Ziolkowski, IEEE Trans. Microwave Theory Tech. **46**, 1628 (1998).
[19] F. Auzanneau and R. W. Ziolkowski, IEEE Trans. Antennas Propag. **47**, 1330 (1999).
[20] H. A. Haus and J. R. Melcher, *Electromagnetic Fields and*

Energy (Prentice Hall, Englewood Cliffs, NJ, 1989).
[21] O. Acher, P. Le Gourriérec, G. Perrin, P. Baclet, and O. Roblin, IEEE Trans. Microwave Theory Tech. **44**, 674 (1996).
[22] J. B. Pendry, A. J. Holden, W. J. Stewart, and I. Youngs, Phys. Rev. Lett. **76**, 4773 (1996).
[23] J. B. Pendry, A. J. Holden, D. J. Robbins, and W. J. Stewart, IEEE Trans. Microwave Theory Tech. **47**, 2075 (1999).
[24] V. G. Veselago, Usp. Fiz. Nauk **92**, 517 (1967) [Sov. Phys. Usp. **10**, 509 (1968)].
[25] D. R. Smith, W. J. Padilla, D. C. Vier, S. C. Nemat-Nasser, and S. Schultz, Phys. Rev. Lett. **84**, 4184 (2000).
[26] R. Fitzgerald, Phys. Today **53** (5), 17 (2000).
[27] R. W. Ziolkowski, IEEE Trans. Antennas Propag. **45**, 656 (1997).
[28] R. W. Ziolkowski, Phys. Rev. E **55**, 7696 (1997).
[29] R. W. Ziolkowski, IEEE Trans. Antennas Propag. **45**, 1530 (1997).
[30] R. W. Ziolkowski, Comput. Methods Appl. Mech. Eng. **169**, 237 (1999).
[31] D.C. Wittwer and R. W. Ziolkowski, IEEE Trans. Antennas Propag. **48**, 192 (2000).
[32] D. C. Wittwer and R. W. Ziolkowski, IEEE Trans. Antennas Propag. **48**, 200 (2000).
[33] R. Donnelly and R. W. Ziolkowski, Proc. R. Soc. London, Ser. A **440**, 541 (1993).
[34] J.-Y. Lu and J. F. Greenleaf, IEEE Trans. Ultrason. Ferroelectr. Freq. Control **39**, 19 (1992).
[35] R. W. Ziolkowski, A. M. Shaarawi, and I. M. Besieris, J. Opt. Soc. Am. A **10**, 75 (1993).
[36] J.-Y. Lu and J. F. Greenleaf, IEEE Trans. Ultrason. Ferroelectr. Freq. Control **39**, 441 (1992).
[37] D. Mugnai, A. Ranfagni, and R. Ruggeri, Phys. Rev. Lett. **84**, 4830 (2000).
[38] R. Y. Chiao, Phys. Rev. A **48**, R34 (1993).
[39] E. L. Bolda and R. Y. Chiao, Phys. Rev. A **48**, 3890 (1993).
[40] A. M. Steinberg and R. Y. Chiao, Phys. Rev. A **49**, 2071 (1994).
[41] E. L. Bolda, J. C. Garrison, and R. Y. Chiao, Phys. Rev. A **49**, 2938 (1994).
[42] R. Y. Chiao and J. Boyce, Phys. Rev. Lett. **73**, 3383 (1994).
[43] R. Y. Chiao, E. Bolda, J. Bowie, J. Boyce, J. C. Garrison, and M. W. Mitchell, Quantum Semiclassic. Opt. **7**, 279 (1995).
[44] L. J. Wang, A. Kuzmich, and A. Dogariu, Nature (London) **406**, 277 (2000).
[45] A. Taflove, *Computational Electrodynamics* (Artech House, Norwood, MA, 1995).
[46] A. Taflove, *Advances in Computational Electrodynamics* (Artech House, Norwood, MA, 1998).
[47] R. W. Ziolkowski and M. Tanaka, J. Opt. Soc. Am. A **16**, 930 (1999).
[48] P. Petropoulis, Applied Mathematics Department, New Jersey Institute of Technology, Newark, NJ, peterp@cams1.njit.edu (private communications).
[49] R. E. Collin, *Field Theory of Guided Waves*, 2nd ed. (IEEE Press, Piscataway, NJ, 1990), pp. 14–17.
[50] L. D. Landau and E. M. Lifshitz, *Electrodynamics of Continuous Media* (Pergamon Press, Oxford, 1960), Sec. 61, pp. 253–256.
[51] R. W. P. King and C. W. Harrison, Jr., *Antennas and Waves: A Modern Approach* (MIT Press, Cambridge, MA, 1969), pp. 60–66.
[52] T. Musha, Proc. IEEE **60**, 1475 (1972).
[53] L. Spruch, Science **272**, 1452 (1996).
[54] G. Plunien, B. Müler, and W. Greiner, Phys. Rep. **134**, 87 (1986).
[55] K. Scharnhorst, Phys. Lett. B **236**, 354 (1990).
[56] G. Barton, Phys. Lett. B **237**, 559 (1990).
[57] P. W. Milonni and K. Svozil, Phys. Lett. B **248**, 437 (1990).
[58] S. Ben-Menahem, Phys. Lett. B **250**, 133 (1990).
[59] P. W. Milonni, *The Quantum Vacuum: An Introduction to Quantum Electrodynamics* (Academic Press, Inc., San Diego, CA, 1994), pp. 249–251.
[60] J. Askne and B. Lind, Phys. Rev. A **2**, 2335 (1970).
[61] J. D. Jackson, *Classical Electrodynamics*, 2nd ed. (John Wiley & Sons, New York, 1975), pp. 160–161.
[62] J. P. Gordon, Phys. Rev. A **8**, 14 (1973).
[63] A. Ashkin, Phys. Rev. Lett. **24**, 156 (1970).
[64] A. P. Kazantsev, Zh. Éksp. Teor. Fiz. **66**, 1599 (1974) [Sov. Phys. JETP **39**, 784 (1974)].
[65] Y. R. Shen, *The Principles of Nonlinear Optics* (John Wiley and Sons, New York, 1984), pp. 368–369.
[66] P. C. Chaumet and M. Nieto-Vesperinas, Opt. Lett. **25**, 1065 (2000).
[67] L. J. Chu, P. H. A. Haus, and P. Penfield, Jr., Proc. IEEE **54**, 920 (1966).
[68] P. Penfield, Jr. and H. A. Haus, *Electrodynamics of Moving Media*, Research Monograph No. 40 (MIT Press, Cambridge, MA, 1967), pp. 48 and 99.